Comparative Study of Global MHD Simulations of the Terrestrial Magnetosphere With Different Numerical Schemes

Yosuke Matsumoto, Naoki Terada, Takahiro Miyoshi, Keiichiro Fukazawa, Takayuki Umeda, Tatsuki Ogino, and Kanako Seki

***Abstract*—We compare recent global MHD simulation models of the terrestrial magnetosphere based on different numerical schemes. The schemes include the finite-difference method based on the modified leapfrog (MLF) scheme, and the semi-Lagrangian scheme based on the constrained interpolation profile (CIP) algorithm. With the two models, we examined the simulation under a northward interplanetary magnetic field (IMF) condition. As a result, we found out that the two simulation models give consistent results on the magnetopause locations at the subsolar point and the terminator, and the overall structures of the cusp in the meridian plane. However, discrepancies are also found in the location and jump conditions of the bow shock. The MLF model showed higher thermal pressure value and weaker magnetic field strength in the downstream than those in the CIP model. The difference in the jump condition across the shock is also reflected in the difference in the length of the magnetotail in the two models. The magnetotail is shorter in the CIP model than that in the MLF model. We conclude that further comparative studies with finite-volume methods are necessary to verify the solution of the bow shock formation and the location of the last closed field line under northward IMF conditions.**

***Index Terms*—Magnetosphere, numerical model, plasma simulation.**

I. Introduction

A GLOBAL MHD simulation of the terrestrial magnetosphere numerically solves an interaction of the magnetosphere with the supersonic solar wind plasma. The first attempt was examined in the 2-D meridian plane by Leboeuf *et al.* [1] more than 30 years ago. Bow shock formation and magnetic reconnection at the dayside magnetopause and in the tail region were successfully shown for the first time in a time-dependent model. Further challenges in 3-D models were examined without [2] and with [3] the interplanetary magnetic field (IMF) in the early 1980s.

Rapid growth of computational capabilities in the last 30 years enables us to simulate more realistic situations of an interaction of transient phenomena of the Sun, such as coronal mass ejections, with the magnetosphere and resultant ionospheric responses such as auroral brightenings. Nowadays, the global MHD simulation is a powerful tool for predicting the geospace environment in response to solar activities, i.e., the space weather forecast. In this context, a number of global MHD simulation models have been developed.

Modern global MHD simulation models numerically solve MHD equations in nonconservative, conservative, or semiconservative forms. The finite-difference method (FDM) is based on the centered finite difference applied to the nonconservative forms of the MHD equations. The advantage of this scheme is its simplicity and low computational costs. The FDM was implemented in earlier models and have been applied to the terrestrial [4][5] and the outer planetary [6] magnetospheres. The drawback of this simple method is that this FDM-based scheme always suffers from spurious oscillations at discontinuities, which require an additional artificial viscosity. Furthermore, the FDM gives inaccurate jump conditions of shocks even with enough spatial resolution [7], [8]. Thus, one needs careful inspections when the FDM is applied to a compressible system.

The full conservative form is well suited for solving the equations by finite-volume methods (FVMs), which ensure conservations of the mass, the momentum, the total energy, and the magnetic flux, and, particularly, accurate jump conditions at shocks. Thus, the FVM is usually adopted for compressible simulations. Recent FVM schemes are combined with an approximate Riemann solver in order to evaluate a numerical flux at cell boundaries, and have been applied to model not only the terrestrial magnetosphere [9], [10] but also other planetary interactions [11].

A drawback of solving in the full conservative form is the difficulty in calculating the thermal pressure in a low-β (a ratio of the thermal pressure to the magnetic pressure) region, where the pressure is obtained by subtracting the large magnetic energy from the total energy; only small errors in the magnetic field result in a negative pressure. This drawback leads to a choice of

Manuscript received December 1, 2009; revised April 30, 2010 and June 21, 2010; accepted June 26, 2010. Date of publication August 5, 2010; date of current version September 10, 2010. This work was supported in part by Grant-in-Aid for JSPS Fellows 08J01791.

Y. Matsumoto, T. Umeda, T. Ogino, and K. Seki are with the Solar–Terrestrial Environment Laboratory, Nagoya University, Nagoya 464-8601, Japan (e-mail: ymatumot@stelab.nagoya-u.ac.jp; umeda@stelab.nagoya-u.ac.jp; ogino@stelab.nagoya-u.ac.jp; seki@stelab.nagoya-u.ac.jp).

N. Terada is with the Department of Geophysics, Graduate School of Science, Tohoku University, Sendai 980-8578, Japan (e-mail: teradan@stpp.gp.tohoku.ac.jp).

T. Miyoshi is with the Department of Physical Science, Graduate School of Science, Hiroshima University, Higashi-Hiroshima 739-8526, Japan (e-mail: miyoshi@sci.hiroshima-u.ac.jp).

K. Fukazawa is with the Department of Earth and Planetary Sciences, Graduate School of Sciences, Kyushu University, Fukuoka 812-8581, Japan (e-mail: fukazawa@geo.kyushu-u.ac.jp).

Color versions of one or more of the figures in this paper are available online at http://ieeexplore.ieee.org.

Digital Object Identifier 10.1109/TPS.2010.2056704

the semiconservative form in which only hydrodynamic quantities are in divergence forms and electromagnetic contributions are added in the momentum and energy equations as source terms. This approach has been successfully implemented in the recent global MHD simulation models [12], [13].

Although numerous models based on different numerical schemes have been developed, they have been tested independently, and they occasionally reach different conclusions even under similar conditions. For example, Raeder [14] reported with his model solved by the semiconservative scheme that the magnetotail does not get closed with low electrical resistivity under a northward IMF condition. Later, Gombosi *et al.* [15] showed similar simulations with their model solved by the fully conservative scheme and indicated that the closed magnetosphere is a universal feature under the northward IMF regardless of the strength of the numerical resistivity. Although some comparative studies have been examined, there has been no direct comparison of different global MHD simulation models under the same solar wind and numerical (e.g., spatial resolutions) conditions. The purpose of this paper is to present a benchmark test of the global MHD simulation by comparing results obtained from different numerical models. This paper is organized as follows. In Section II, we describe the numerical schemes, solar wind conditions, and simulation settings used for the benchmark test. In Section III, we compare the obtained simulation results based on the different numerical schemes by focusing on the positions of discontinuities, jump conditions at the bow shock, and their spatial resolutions. The differences found in the present comparative study are discussed in the last section.

II. Numeric

In this paper, we adopt an FDM based on the modified leapfrog (MLF) method, and the semi-Lagrangian method based on the constrained interpolation profile (CIP) algorithm for the comparative study of the global MHD simulation.

A. Modified Leapfrog Scheme

The MLF scheme is developed by Ogino *et al.* [4]. The scheme is based on a combination of the leapfrog scheme and the two-step Lax–Wendroff scheme. For example, the MLF solves an equation

$$\frac{\partial f}{\partial t} = \frac{\partial u}{\partial x} \tag{1}$$

by differentiating the right-hand side centered in time and space as

$$\frac{f_i^{n+1} - f_i^n}{\Delta t} = \frac{u_{i+1/2}^{n+1/2} - u_{i-1/2}^{n+1/2}}{\Delta x} \tag{2}$$

where n refers to a time step and i refers to a spatial grid point. The half-time step value ($u^{n+1/2}$ on the right-hand side) is obtained by the two-step Lax-Wendroff scheme. The two-step Lax-Wendroff scheme is used for one time step and then the leapfrog scheme is applied for $(l-1)$ time steps. Here, l is arbitrary and is usually adopted as eight. The MLF scheme reduces numerical phase errors and numerical damping in comparison with the two-step Lax-Wendroff scheme without introducing large computational costs.

The MLF scheme solves the MHD equations in nonconservative forms as

$$\frac{\partial \rho}{\partial t} = -(\mathbf{V}\cdot\nabla)\rho - \rho(\nabla\cdot\mathbf{V}) \tag{3}$$

$$\frac{\partial \mathbf{V}}{\partial t} = -(\mathbf{V}\cdot\nabla)\mathbf{V} - \frac{1}{\rho}\nabla P + \frac{1}{\rho}(\mathbf{J}\times\mathbf{B}) \tag{4}$$

$$\frac{\partial P}{\partial t} = -(\mathbf{V}\cdot\nabla)P - \Gamma P(\nabla\cdot\mathbf{V}) \tag{5}$$

$$\frac{\partial \mathbf{B}}{\partial t} = -\boldsymbol{\nabla}\times\mathbf{E} = \boldsymbol{\nabla}\times\left(\frac{\mathbf{V}}{c}\times\mathbf{B}\right) \tag{6}$$

$$\mathbf{J} = \frac{c}{4\pi}\nabla\times(\mathbf{B}-\mathbf{B_d}) \tag{7}$$

where ρ, $\mathbf{V}$, P, Γ, $\mathbf{B}$, $\mathbf{E}$, c, and $\mathbf{J}$ denote the mass density, the velocity, the thermal pressure, the specific heat ratio set as 5/3, the magnetic field, the electric field, the speed of light, and the current density, respectively. $\mathbf{B}_d$ is the background dipole magnetic field of the Earth, which is a force-free field and therefore does not contribute to the current density (7). In addition to the basic equations, diffusion terms are added to the equations of continuity (3), motion (4), and state (5) in order to suppress numerical oscillations at discontinuities. Also, the resistive term is added to the induction equation of the magnetic field (6).

B. Semi-Lagrangian Scheme

The semi-Lagrangian scheme is the method that solves an advection equation by reconstructing a profile in the upwind direction. The CIP scheme [16] is one of those schemes, and it has shown high performance in solving the advection equation with small numerical phase errors. The CIP scheme follows time developments of spatial derivatives as well as a physical quantity f itself as

$$\frac{\partial f}{\partial t} = -\mathbf{V}\cdot\nabla f \tag{8}$$

$$\frac{\partial \mathbf{g}}{\partial t} = -\mathbf{V}\cdot\nabla\mathbf{g} \tag{9}$$

where $\mathbf{V}$ is the advection speed vector and

$$\mathbf{g} = \boldsymbol{\nabla} f = \begin{pmatrix} \partial f/\partial x \\ \partial f/\partial y \\ \partial f/\partial z \end{pmatrix}. \tag{10}$$

A profile of the physical quantity in the upwind direction is reconstructed by the third-order polynomial. For a 1-D problem in the x-direction with $V_x > 0$, for example, the profiles for f and g are reconstructed as

$$F(X) = c_3X^3 + c_2X^2 + c_1X + c_0 \tag{11}$$

$$G(X) = \frac{\partial F}{\partial X} = 3c_3X^2 + 2c_2X + c_1 \tag{12}$$

where X is an upwind distance from a grid point x_i. The coefficients c_0, c_1, c_2, and c_3 are determined from conditions

$$F(0) = f(x_i) \tag{13}$$

$$F(x_i - x_{i-1}) = f(x_{i-1}) \tag{14}$$

$$G(0) = g(x_i) \tag{15}$$

$$G(x_i - x_{i-1}) = g(x_{i-1}). \tag{16}$$

Then, f and g are updated as

$$f^{n+1} = F(x_i - V_x \Delta t) \tag{17}$$

$$g^{n+1} = G(x_i - V_x \Delta t). \tag{18}$$

In applying the CIP scheme to (magneto) hydrodynamical equations, the terms are separately solved by advection and nonadvection phases. The nonadvection phase is usually solved by an FDM. The CIP scheme has been applied to solve the advection term in the MHD equations for space [17], [18] and astrophysical [19] phenomena.

In applying the CIP scheme to the MHD equations, Matsumoto and Seki [20] recently showed an alternative way by solving the equations in unfamiliar forms based on Elsässer variables [21], [22]

$$\frac{\partial \mathbf{Z}^{\pm}}{\partial t} + \mathbf{Z}^{\mp} \cdot \boldsymbol{\nabla} \mathbf{Z}^{\pm} = -\frac{1}{\rho} \boldsymbol{\nabla} P_t + \frac{\mathbf{V_A}}{2\rho} (\mathbf{V_A} \cdot \boldsymbol{\nabla}) \rho \mp \frac{\mathbf{V_A}}{2} (\boldsymbol{\nabla} \cdot \mathbf{V}) \tag{19}$$

where

$$\mathbf{Z}^{\pm} = \mathbf{V} \pm \mathbf{V_A} \tag{20}$$

$$\mathbf{V_A} = \frac{\mathbf{B}}{\sqrt{4\pi\rho}} \tag{21}$$

$$P_t = P + \frac{\rho V_A^2}{2}. \tag{22}$$

The left-hand side of (19) is the advective part, which is solved by the CIP scheme. By solving the advection equation in terms of Elsässer variables, the CIP scheme gives highly accurate solutions to Alfvén-wave propagation and the advective motion [20]. The right-hand side of (19) consists of the total (thermal and magnetic) pressure gradient term (the first term) and the compressional terms (the last two terms), which are related to the compressional (fast and slow) waves and solved as the nonadvective phase by the third-order Adams–Moulton predictor-corrector method. In this paper, we used this method by employing the R-CIP scheme [23], which replaces the third-order polynomial by a rational function to ensure monotonicity at discontinuities. In the present global MHD simulation code, we solved the equation for the perturbed value of $\delta \mathbf{Z}^{\pm} = \delta \mathbf{V} \pm \delta \mathbf{V_A}$, where $\delta \mathbf{V_A} = (\mathbf{B}/\sqrt{4\pi\rho} - \mathbf{B_d}/\sqrt{4\pi\rho_0})$, with ρ_0 being the initial equilibrium mass density.

While the (R-)CIP scheme well resolves the contact and tangential discontinuities within a few grid points, it does not provide accurate solutions to shock formation. In order to correctly solve the bow shock formation in front of the magnetosphere, we introduced the shock-capturing artificial viscosity [24], which has been successfully implemented for a high-Mach-number solar wind ($M_f \sim 10$) interaction with the planet Mercury's magnetosphere [18]. Small viscosity and resistivity are also added to (19).

C. Simulation Parameters and Boundary Conditions

We adopt the solar wind parameters of Ogino *et al.* [4]; a solar wind plasma of $n_{\rm sw} = 5.0$ cm^{-3}, $V_{\rm sw} = 300.0$ km $\cdot$ s^{-1}, and $T_{\rm sw} = 2.0 \times 10^5$ K is injected into a simulation box at $X = -45\ R_E$, where $R_E = 6380$ km is the Earth's radius. The simulation box ranges in $-45\ R_E \le X \le +135\ R_E$, $-45\ R_E \le Y \le 0$, and $0 \le Z \le +45\ R_E$ and thus covers the north-dusk sector of the magnetosphere. In addition to the plasma parameters, we induce a northward IMF of $B_z = +5.0$ nT for the present benchmark test.

The initial equilibrium is maintained by the Earth's dipole magnetic field, whose strength on the Earth's equatorial surface is 3.108×10^4 nT, and the plasma number density of $n_0 = 0.2 n_{\rm sw}$ and the temperature of $T_0 = T_{\rm sw}$ are uniformly distributed in the simulation box.

The equations are discretized in a uniform regular Cartesian grid system for the MLF scheme and in a uniform staggered Cartesian grid system for the CIP scheme. The spatial resolution is $\Delta h = 0.3\ R_E$. Thus, the number of cells in each direction is $(N_x, N_y, N_z) = (600, 150, 150)$. The time step sizes are $\Delta t = 0.21$ (s) for the MLF scheme and $\Delta t = 0.052$ (s) for the CIP scheme.

Open-boundary conditions are applied in the planes at $X = +135\ R_E$, $Y = -45\ R_E$, and $Z = +45\ R_E$. Mirror boundary conditions are applied at the meridian and equatorial planes so that symmetric solutions are obtained at the boundaries. We also applied fixed boundary conditions in the region $R < 5\ R_E$, where R is a radial distance from the Earth's position. Some special treatments are necessary to suppress numerical oscillations near the inner boundary at $R = 5\ R_E$. In the models, some smoothing techniques (e.g., [4]), which do not severely affect the outer magnetospheric dynamics, are applied in the region $5\ R_E \le R \le 7\ R_E$ for the MLF scheme and in the region $5\ R_E \le R \le 6\ R_E$ for the CIP scheme.

III. Results

We compare the results of the interaction of the magnetosphere with the solar wind by the global MHD simulations based on the MLF and CIP schemes. The solar wind plasma is continuously injected into the simulation box for 4 h. For the northward IMF condition, we expect the formation of a compact closed magnetosphere as a result of the tailward-of-the-cusp reconnection between the IMF and the Earth's intrinsic magnetic field (e.g., [25]).

Fig. 1 shows 3-D views of the magnetospheric responses to the injected solar wind plasma for the MLF (left column) and the CIP (right column) models. As a result of the interaction of the supersonic flow with an obstacle, the fast (bow) shock is formed in front of the magnetosphere in both cases [Fig. 1(a) and (e)]. The intrinsic magnetic field is stretched by the solar wind, forming the magnetotail in the nightside. After calculating for 2 h, a compact closed magnetosphere is formed in

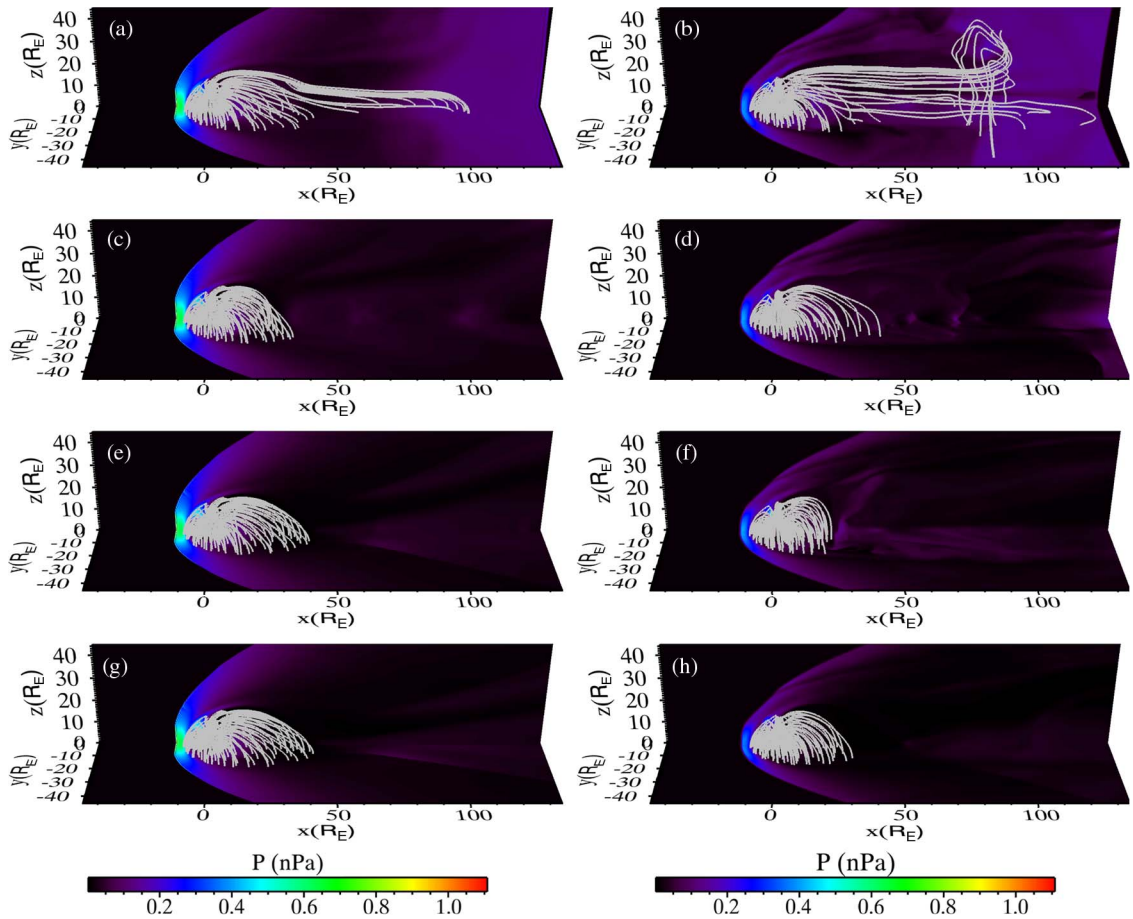

Fig. 1. Three-dimensional views of the interaction of the magnetosphere with the solar wind plasma for (a–d) the MLF and (e–h) the CIP models. The spatial profiles of the thermal pressure in the equatorial and meridian planes are color-coded in the unit of nanopascals. The solid lines are the magnetic field lines closed into the Earth. Snapshots are taken at (a, e) 1 h, (b, f) 2 h, (c, g) 3 h, and (d, h) 4 h from the beginning.

both models [Fig. 1(b) and (f)]. The flow behind the magnetosphere is laminar in the MLF model, while it is somewhat turbulent in the CIP model. Three hours from the beginning, the magnetosphere achieved a quasi-steady state in the MLF model [Fig. 1(c)], while the shape of the magnetosphere is deformed by the fast returning flows behind the magnetosphere in the CIP model [Fig. 1(g)]. (Note that the returning flows are not due to the magnetic reconnection in the tail but are due to the open-boundary condition at $X = 135R_E$.) In the final state after 4 h, the magnetosphere achieved a steady state in the CIP model [Fig. 1(h)], which is more compact than the MLF model [Fig. 1(d)].

From Fig. 1, we found out that the two models show a similar overall structure of the magnetosphere under the same solar wind conditions. A closer look at the equatorial plane, however, shows different shapes of the bow shock and flow patterns. Fig. 2 shows the spatial profiles of the pressure and the flow vectors in the equatorial plane taken 4 h from the beginning [same snapshots as Fig. 1(d) and (h)]. The shape of the bow shock is rectangular at the nose in the MLF model, while the CIP model shows a smooth arc shape. We plotted the pressure, the density, the x-component of the velocity, and the z-component of the magnetic field profiles across the subsolar point $(Y = Z = 0)$ in Fig. 3. In the MLF model (black line), the bow shock is located at $X = -14\ R_E$, where spurious oscillations are found

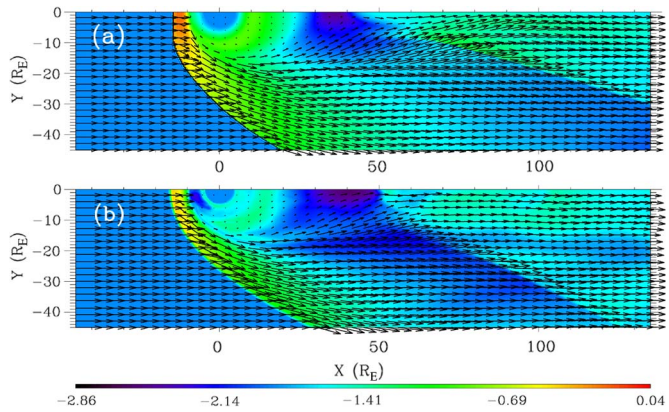

Fig. 2. Spatial profiles of the thermal pressure color-coded in a logarithmic scale and the flow vectors in the equatorial plane are shown for the (a) MLF and (b) CIP models.

in all physical quantities. In the CIP model, the bow shock is located at $X = -15.5\ R_E$. The discontinuous changes in all variables are captured with a few grid points in the CIP model. Thus, there is a large discrepancy in the shock location between the two models. The pressure in the downstream of the shock in the MLF model is twice as large as that in the CIP model, while the z-component of the magnetic field is larger in the CIP model than that in the MLF model. The number density in the

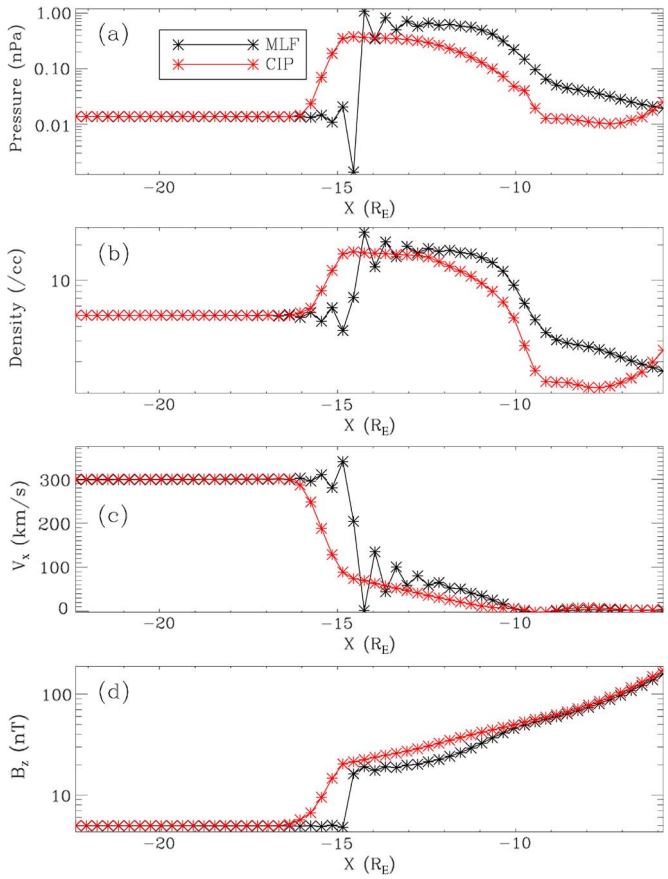

Fig. 3. Line plots of (a) the thermal pressure, (b) the number density, (c) the x-component of the velocity, and (d) the z-component of the magnetic field across the subsolar point ($Y = Z = 0$). The black and red lines show for the MLF and CIP models, respectively.

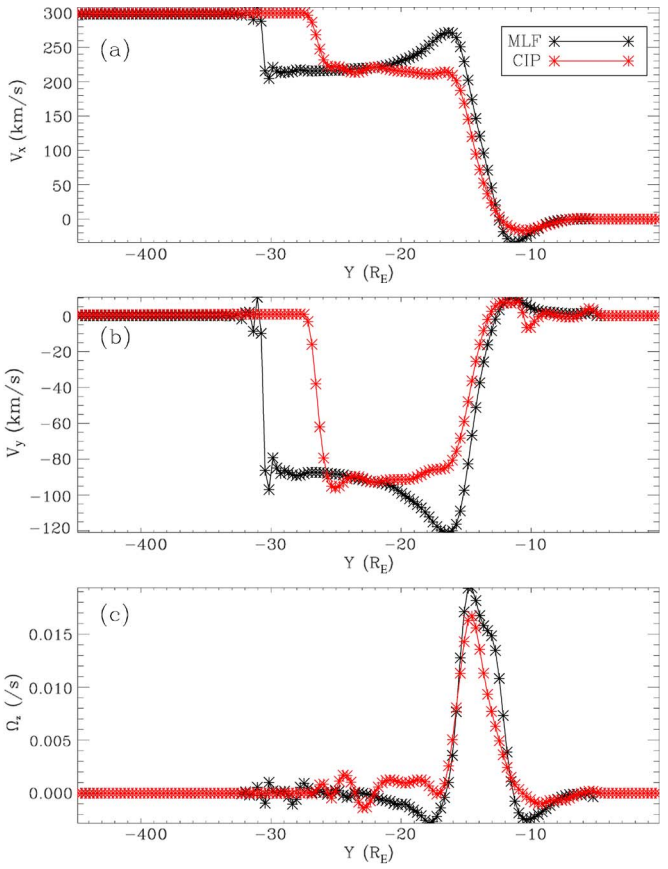

Fig. 4. Line plots of (a) the x- and (b) y-components of the velocity, and (c) the z-component of the vorticity along the terminator ($X = Z = 0$). The black and red lines show for the MLF and CIP models, respectively.

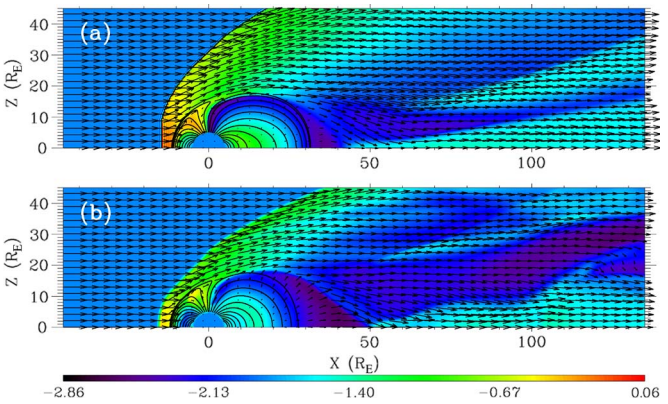

Fig. 5. Spatial profiles of the thermal pressure color-coded in a logarithmic scale, the flow vectors, and the magnetic field lines closed into the Earth (black solid lines) in the meridian plane are shown for the (a) MLF and (b) CIP models.

downstream consistently shows $N \sim 20$ cm^{-3} in both models. From the spatial variation in the number density, the dayside magnetopause is found to be located at $X = -10\ R_E$ in both simulation models. Contrary to the bow shock location, the magnetopause location is in good agreement with each other.

Fig. 4 shows the spatial profiles of the x- and y-components of the velocity, and the z-component of the vorticity calculated from $\Omega_z = \nabla \times \mathbf{V}|_z = \partial V_y/\partial x - \partial V_x/\partial y$ along the terminator ($X = Z = 0$). From the profiles of the x- and y-components of the velocity, we found out that the bow shock is located at $Y = -31\ R_E$ in the MLF model and at $Y = -26\ R_E$ in the CIP model. We meet again a large difference in the bow shock location between the two models. In the magnetosheath, the flow speeds in both models are $V_x \sim 210$ km $\cdot$ s^{-1} and $V_y \sim -90$ km $\cdot$ s^{-1}, showing consistent results with each other. In Fig. 4(c), we show the vorticity profile in order to examine a location of the velocity shear layer across at the magnetopause. We found out that the width of the velocity shear is thinner in the CIP model than that in the MLF model, while the location of the peak value is at $Y = -15\ R_E$ in both simulation models, which shows consistent results with each other, as shown for the subsolar point.

In the meridian plane, we compare the cusp location and the shape of the magnetotail. Fig. 5 shows the spatial profiles of the thermal pressure, the flow vectors, and the field lines of the intrinsic magnetic field (closed field lines). While the overall structure of the cusp region is consistent in the two simulation models, the pressure in the MLF model is higher than that in the CIP model. This difference in pressure value is attributed to the difference in the jump condition across the bow shock, as shown in Fig. 3. As the solar wind plasma flows past the magnetosphere, a rarefaction region is formed behind the magnetosphere, which is also shown in the equatorial plane (Fig. 2). The last closed magnetic field line is located at $X = +32\ R_E$ in the MLF model and at $X = +28\ R_E$ in the CIP model. The CIP model gives a more compact magnetosphere.

TABLE I
LOCATIONS OF BOUNDARIES

	Bow shock	Magnetopause (dayside)	Magnetopause (dusk)	Last closed field line
MLF	-14 R_E	-10 R_E	-15 R_E	+32 R_E
CIP	-15.5 R_E	-10 R_E	-15 R_E	+28 R_E

The locations of the identified boundaries are summarized in Table I.

IV. SUMMARY AND DISCUSSION

We have compared global MHD simulation models of the terrestrial magnetosphere based on the FDM of the MLF scheme and the semi-Lagrangian CIP scheme. Under a northward IMF condition, the two simulation models showed consistent results on the magnetopause locations at the subsolar point and the terminator, and the overall structure of the cusp in the meridian plane.

Discrepancies were, however, found in the location and jump conditions of the bow shock. It is well known that FDMs give inaccurate jump conditions of shocks even with enough spatial resolutions [7], [8]. Since the equations are solved in nonconservative forms, the MLF model is subject to this problem. The same can be true for the CIP model, in which the equations are solved in nonconservative forms, unless the shock-capturing artificial viscosity is introduced. In the CIP model, supplemental pressure is added in the equations of motion and state so as to satisfy the Rankine–Hugoniot relation, giving more accurate solutions to the shock formation [24], [26], [27].

We found out by both models that the last closed field line is located around $X = +30\ R_E$ in the nightside of the magnetosphere. Song *et al.* [28] studied comprehensively the locations of the last closed field line (tail length) for various northward IMF and solar wind parameters. For IMF $B_z = +5$ nT, a solar wind number density of 5.0 cm^{-3}, and a speed of 400 $\mathrm{km \cdot s^{-1}}$, the field line is closed at $56R_E$ in the nightside. From the other results for those parameters listed by Gombosi *et al.* [15], the location of the last closed field line ranges around $50R_E$ in the nightside of the magnetosphere, which is farther than the location obtained in this paper. It was also reported that the tail length is determined by the viscous interaction with the solar wind and the pressure gradient force from the dayside to the nightside of the magnetosphere. The former is clearly related to the solar wind (magnetosheath) speed. The latter was found to be related to $\sqrt{1+\beta}+1$ in the magnetosheath near the subsolar point [25]. Thus, the magnetosonic Mach number of the solar wind is also a determining factor for the tail length. Since the solar wind speed of 300 $\mathrm{km \cdot s^{-1}}$ is adopted, the shorter tail length obtained in this paper ($\sim 30\ R_E$) is a natural consequence for the slower and lower Mach number solar wind.

We also note a slight difference in the tail length between the MLF ($32\ R_E$) and CIP ($28\ R_E$) models. In the MLF model, the thermal pressure in the downstream of the shock (magnetosheath) is twice as large as that in the CIP model, as shown in Fig. 3. This difference in the jump condition across the bow shock affects the beta value in the magnetosheath near the subsolar point, which is closely related to the length of the magnetotail, as previously discussed. Since the tail length linearly increases as $\sqrt{1+\beta}+1$ in the magnetosheath increases [28], the longer tail in the MLF model can be attributed to the higher pressure value and lower magnetic field strength in the magnetosheath in the MLF model. There also has been a debate on the effect of electrical resistivity on tail length [14], [15]. Since the numerical resistivity is inherent to each numerical model, the effect of resistivity on the location of the last closed field line is not clearly understood by limited simulation runs in this paper.

In summary, while similar overall structures of the magnetosphere under a northward IMF condition are obtained, the MLF and CIP models gave different solutions to the location of the bow shock and the thermal pressure and the magnetic field strength in the downstream near the subsolar point, which may lead to different sizes of the magnetotail. Thus, further verifications are necessary with FVMs, which accurately solve conservation laws across shocks. Comparison with the FVM based on the HLLD Riemann solver [29] is to be done in the near future. In addition, we are planning to benchmark global MHD simulation models under a southward IMF condition to compare, particularly, the location of magnetic reconnection in the magnetotail.

ACKNOWLEDGMENT

The computational resources are provided by NEC SX9 at JAXA's Engineering and Digital Innovation Center, Japan Aerospace Exploration Agency (JAXA), Japan, and NEC SX8 at the National Institute of Information and Communications Technology (NICT), Japan.

REFERENCES

[1] J. N. Leboeuf, T. Tajima, C. F. Kennel, and J. M. Dawson, "Global simulation of the time-dependent magnetosphere," *Geophys. Res. Lett.*, vol. 5, no. 7, pp. 609–612, Jul. 1978.

[2] C. C. Wu, R.J. Walker, and J. M. Dawson, "A three dimensional MHD model of the Earth's magnetosphere," *Geophys. Res. Lett.*, vol. 8, no. 5, pp. 523–526, May 1981.

[3] T. Ogino, "A three-dimensional MHD simulation of the interaction of the solar wind with the Earth's magnetosphere: The generation of field-aligned currents," *J. Geophys. Res.*, vol. 91, no. A6, pp. 6791–6806, Jun. 1986.

[4] T. Ogino, R. J. Walker, and M. Ashour-Abdalla, "A global magnetohydrodynamic simulation of the magnetosheath and magnetosphere when the interplanetary magnetic field is northward," *IEEE Trans. Plasma Sci.*, vol. 20, no. 6, pp. 817–828, Dec. 1992.

[5] K. S. Park, T. Ogino, and R. J. Walker, "On the importance of antiparallel reconnection when the dipole tilt and IMF $\mathrm{B_y}$ are nonzero," *J. Geophys. Res.*, vol. 111, no. A5, p. A05 202, May 2006.

[6] K. Fukazawa, T. Ogino, and R. J. Walker, "Configuration and dynamics of the Jovian magnetosphere," *J. Geophys. Res.*, vol. 111, no. A10, p. A10 207, Oct. 2006.

[7] P. D. Lax and B. Wendroff, "Systems of conservation laws," *Commun. Pure Appl. Math.*, vol. 13, pp. 217–237, 1960.

[8] T. Y. Hou and P. G. LeFloch, "Why nonconservative schemes converge to wrong solutions: Error analysis," *Math. Comput.*, vol. 62, no. 206, pp. 497–530, Apr. 1994.

[9] T. Tanaka, "Finite volume TVD scheme on an unstructured grid system for three-dimensional MHD simulation of inhomogeneous systems including strong background potential fields," *J. Comput. Phys.*, vol. 111, no. 2, pp. 381–389, Apr. 1994.
[10] T. I. Gombosi, K. G. Powell, D. L. Dezeeuw, C. R. Clauer, K. C. Hansen, W. B. Manchester, A. J. Ridley, I. I. Roussev, I. V. Sokolov, and Q. F. Stout, "Solution-adaptive magnetohydrodynamics for space plasmas: Sun-to-Earth simulations," *Comput. Sci. Eng.*, vol. 6, no. 2, pp. 14–35, Mar. 2004.
[11] N. Terada, H. Shinagawa, T. Tanaka, K. Murawski, and K. Terada, "A three-dimensional, multispecies, comprehensive MHD model of the solar wind interaction with the planet Venus," *J. Geophys. Res.*, vol. 114, no. A9, p. A09 202, Sep. 2009.
[12] J. G. Lyon, J. A. Fedder, and C. M. Modarry, "The Lyon–Fedder–Mobarry (LFM) global MHD magnetospheric simulation code," *J. Atmos. Sol.-Terr. Phys.*, vol. 66, no. 15/16, pp. 1333–1350, Oct. 2004.
[13] J. Raeder, D. Larson, W. Li, E. L. Kepko, and T. Fuller-Rowell, "OpenGGCM simulations for the THEMIS mission," *Space Sci. Rev.*, vol. 141, no. 1–4, pp. 535–555, Dec. 2008.
[14] J. Raeder, "Modeling the magnetosphere for northward interplanetary magnetic field: Effects of electrical resistivity," *J. Geophys. Res.*, vol. 104, no. A8, pp. 17 357–17 367, Aug. 1999.
[15] T. I. Gombosi, K. G. Powell, and B. van Leer, "Comment on 'modeling the magnetosphere for northward interplanetary magnetic field: Effects of electrical resistivity' by Joachim Raeder," *J. Geophys. Res.*, vol. 105, no. A6, pp. 13 141–13 147, Jun. 2000.
[16] T. Yabe, F. Xiao, and T. Utsumi, "The constrained interpolation profile method for multiphase analysis," *J. Comput. Phys.*, vol. 169, no. 2, pp. 556–593, May 2001.
[17] Y. Matsumoto and K. Seki, "The secondary instability initiated by the three-dimensional nonlinear evolution of the Kelvin–Helmholtz instability," *J. Geophys. Res.*, vol. 112, p. A06 223, Jun. 2007.
[18] M. Yagi, K. Seki, and Y. Matsumoto, "Development of a magnetohydrodynamic simulation code satisfying the solenoidal magnetic field condition," *Comput. Phys. Commun.*, vol. 180, no. 9, pp. 1550–1557, Sep. 2009.
[19] T. Kudoh, R. Matsumoto, and K. Shibata, "Magnetically driven jets from accretion disks. III. 2.5-dimensional nonsteady simulations for thick disk case," *Astrophys. J.*, vol. 508, pp. 186–199, 1998.
[20] Y. Matsumoto and K. Seki, "Implementation of the CIP algorithm to magnetohydrodynamic simulations," *Comput. Phys. Commun.*, vol. 179, no. 5, pp. 289–296, Sep. 2008.
[21] W. M. Elsässer, "The hydromagnetic equations," *Phys. Rev.*, vol. 79, no. 1, p. 183, 1950.
[22] E. Marsch and A. Mangeney, "Ideal MHD equations in terms of compressive Elsässer variables," *J. Geophys. Res.*, vol. 92, pp. 7363–7367, Jul. 1987.
[23] F. Xiao, T. Yabe, G. Nizam, and T. Ito, "Constructing a multi-dimensional oscillation preventing scheme for the advection equation by a rational function," *Comput. Phys. Commun.*, vol. 94, no. 2/3, pp. 103–119, Apr. 1996.
[24] Y. Ogata and T. Yabe, "Shock capturing with improved numerical viscosity in primitive Euler representation," *Comput. Phys. Commun.*, vol. 119, no. 2/3, pp. 179–193, Jun. 1999.
[25] P. Song and C. T. Russell, "Model of the formation of the low-latitude boundary layer for strongly northward interplanetary magnetic field," *J. Geophys. Res.*, vol. 97, no. A2, pp. 1411–1420, Feb. 1992.
[26] M. L. Wilkins, "Use of artificial viscosity in multidimensional fluid dynamic calculations," *J. Comput. Phys.*, vol. 36, pp. 281–303, Jul. 1980.
[27] T. D. Arber, A. W. Longbottom, C. L. Gerrard, and A. M. Milne, "A staggered grid, Lagrangian–Eulerian remap code for 3-D MHD simulations," *J. Comput. Phys.*, vol. 171, no. 1, pp. 151–181, Jul. 2001.
[28] P. Song, D. L. DeZeeuw, T. I. Gombosi, C. P. T. Groth, and K. G. Powell, "A numerical study of solar wind-magnetosphere interaction for northward interplanetary magnetic field," *J. Geophys. Res.*, vol. 104, no. A12, pp. 28 361–28 378, 1999.
[29] T. Miyoshi and K. Kusano, "A multi-state HLL approximate Riemann solver for ideal magnetohydrodynamics," *J. Comput. Phys.*, vol. 208, no. 1, pp. 315–344, Sep. 2005.

Yosuke Matsumoto received the Ph.D. degree from the University of Tokyo, Tokyo, Japan, in 2004.

He was a COE Research Fellow at the Graduate School of Environmental Studies, Nagoya University, Nagoya, Japan, from 2004 to 2008. Since 2008, he has been with the Solar–Terrestrial Environment Laboratory, Nagoya University, Nagoya, Japan, as a JSPS Research Fellow. His research interests include numerical simulations with applications in space plasma physics.

Naoki Terada received the Ph.D. degree from Kyoto University, Kyoto, Japan, in 2002.

He was a Postdoctoral Fellow at the Solar–Terrestrial Environment Laboratory, Nagoya University, Nagoya, Japan, from 2002 to 2005 and then as a JST-CREST Postdoctoral Fellow at the National Institute of Information and Communications Technology, Koganei, Japan, from 2005 to 2009. Since 2009, he has been with the Department of Geophysics, Graduate School of Science, Tohoku University, Sendai, Japan, as an Associate Professor. His research interests include numerical simulations with applications in space plasma physics.

Takahiro Miyoshi received the Ph.D. degree from Hiroshima University, Higashi-Hiroshima, Japan, in 1998.

He was a Postdoctoral Fellow at the Naka Fusion Research Establishment, Japan Atomic Energy Research Institute, Naka, Japan, from 1998 to 2001. Since 2001, he has been with the Department of Physical Science, Graduate School of Science, Hiroshima University, Higashi-Hiroshima, as an Assistant Professor. His research interests include computational magneto-fluid dynamics and its applications in plasma physics.

Keiichiro Fukazawa received the Ph.D. degree from Nagoya University, Nagoya, Japan, in 2007.

He was a Postdoctoral Fellow at the National Institute of Information and Communications Technology, Koganei, Japan, from 2007 to 2009. Since 2009, he has been with the Department of Earth and Planetary Sciences, Graduate School of Sciences, Kyushu University, Fukuoka, Japan, as a JSPS Research Fellow. His research interests include computational magnetohydrodynamics and its application in plasma physics.

Takayuki Umeda received the Ph.D. degree from Kyoto University, Kyoto, Japan, in 2004.

He was a Postgraduate Researcher with the Institute of Geophysics and Planetary Physics, University of California, Los Angeles, from 2004 to 2006. Since 2006, he has been with the Solar–Terrestrial Environment Laboratory, Nagoya University, Nagoya, Japan, as an Assistant Professor. His research interests include computational sciences and high-performance computing with applications in space plasma physics.

Tatsuki Ogino received the Ph.D. degree from Nagoya University, Nagoya, Japan, in 1976.

He joined the Department of Electrical Engineering, Nagoya University, in 1976 as a Research Associate. He moved to the Solar–Terrestrial Environment Laboratory, Nagoya University, in 1978, where he was appointed as Professor in 1996. His main research interests include terrestrial and planetary magnetospheric physics and magnetohydrodynamic simulations.

Kanako Seki received the Ph.D. degree from the University of Tokyo, Tokyo, Japan, in 2000.

She was a Research Fellow for the Japan Society for the Promotion of Science at the University of Tokyo from 2000 to 2002. Since 2002, she has been with the Solar–Terrestrial Environment Laboratory, Nagoya University, Nagoya, Japan, as an Associate Professor. Her research interests include plasma universe, geospace environment, and comparative planetary magnetospheres.